JACS JOURNAL OF THE AMERICAN CHEMICAL SOCIETY

Article

Cite This: J. Am. Chem. Soc. 2018, 140, 14878−14886

pubs.acs.org/JACS

The Phosphine Oxide Route toward Lead Halide Perovskite Nanocrystals

Guilherme Almeida,[†,▽] Olivia J. Ashton,[§,▽] Luca Goldoni,[‡] Daniela Maggioni,[∥] Urko Petralanda,[†] Nimai Mishra,[†,&] Quinten A. Akkerman,[†,⊥] Ivan Infante,[#] Henry J. Snaith,[§] and Liberato Manna*[,†]

[†]Department of Nanochemistry and [‡]Analytical Chemistry Facility, Istituto Italiano di Tecnologia, Via Morego 30, 16163 Genova, Italy

[§]Clarendon Laboratory, Department of Physics, University of Oxford, Parks Road, OX1 3PU, Oxford, U.K.

[∥]Dipartimento di Chimica, Università degli Studi di Milano, Via Golgi 19, 20133 Milano, Italy

[⊥]Dipartimento di Chimica e Chimica Industriale, Università degli Studi di Genova, Via Dodecaneso 31, 16146 Genova, Italy

[#]Department of Theoretical Chemistry, Faculty of Science, Vrije Universiteit Amsterdam, de Boelelaan 1083, 1081 HV Amsterdam, The Netherlands

Supporting Information

ABSTRACT: We report an amine-free synthesis of lead halide perovskite (LHP) nanocrystals, using trioctylphosphine oxide (TOPO) instead of aliphatic amines, in combination with a protic acid (e.g., oleic acid). The overall synthesis scheme bears many similarities to the chemistry behind the preparation of LHP thin films and single crystals, in terms of ligand coordination to the chemical precursors. The acidity of the environment and hence the extent of protonation of the TOPO molecules tune the reactivity of the PbX_2 precursor, regulating the size of the nanocrystals. On the other hand, TOPO molecules are virtually absent from the surface of our nanocrystals, which are simply passivated by one type of ligand (e.g., Cs-oleate). Furthermore, our studies reveal that Cs-oleate is dynamically bound to the surface of the nanocrystals and that an optimal surface coverage is critical for achieving high photoluminescence quantum yield. Our scheme delivers NCs with a controlled size and shape: only cubes are formed, with no contamination with platelets, regardless of the reaction conditions that were tested. We attribute such a shape homogeneity to the absence of primary aliphatic amines in our reaction environment, since these are known to promote the formation of nanocrystals with sheet/platelet morphologies or layered phases under certain reaction conditions. The TOPO route is particularly appealing with regard to synthesizing LHP nanocrystals for large-scale manufacturing, as the yield in terms of material produced is close to the theoretical limit: i.e., almost all precursors employed in the synthesis are converted into nanocrystals.

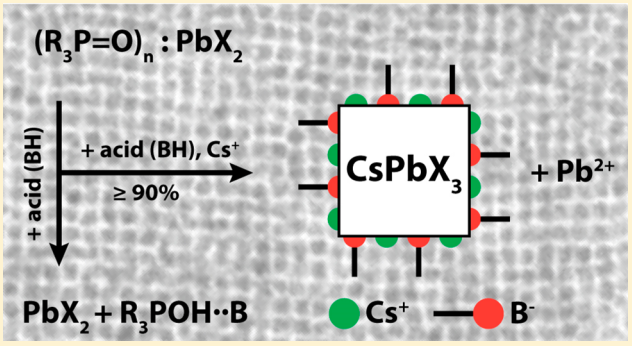

INTRODUCTION

Lead halide perovskites (LHPs), with the general formula $APbX_3$ (A = CH_3NH_3, Cs, etc.; X = Cl, Br, I), are a class of gap-tunable semiconductors ($1.4 \leq E_g \leq 2.9$ eV) that has been intensively investigated over the past decade and holds great promise for applications in solution-processed photonic and optoelectronic technologies.[1−5] As LHP thin film solar cells are attaining record power conversion efficiencies and the performance of light-emitting diodes based on nanocrystalline LHP films is approaching commercial values, considerable work has been devoted to improving and optimizing the fabrication and stability of materials[6−13] and devices.[2,14−18] Large-grain (>100 nm) LHP crystals and thin films are typically fabricated using polar solvents, such as dimethyl sulfoxide (DMSO), dimethylformamide (DMF), and γ-butyrolactone (GBL), all of which have carbonyl or thionyl (RX═O; X = C, S) groups.[1,6,10] Conversely, LHP nanocrystals (NCs) are fabricated in nonpolar solvents employing a mixture of aliphatic primary amines and carboxylic acids to solvate PbX_2. While these polar solvents are not appropriate for industrial-scale synthesis due to toxicity concerns,[19−21] the presence of primary amines in the NC synthesis is also not ideal. In the synthesis of $APbX_3$ NCs, primary amines (usually oleylamine) are found in equilibrium with their protonated form, alkylammonium ions, which compete with A cations for the same lattice sites and promote the formation of nanosheets/nanoplatelets or even layered phases.[12] Furthermore, this route provides NCs with a complex and dynamic ligand shell,[22] and the synthesis of monodisperse LHP NCs

Received: August 20, 2018
Published: October 25, 2018

DOI: 10.1021/jacs.8b08978
J. Am. Chem. Soc. 2018, 140, 14878−14886

with high yields has yet to be demonstrated. Finally, several works have shown that amines can drive the dissolution of LHPs and their transformation into an insulating phase.[12,23,24]

In this work, we study the synthesis of $CsPbBr_3$ NCs (a model LHP in terms of composition) using trioctylphosphine oxide ($(C_8H_{17})_3P{=}O$, TOPO) and oleic acid (OA), and we avoid the use of aliphatic amines. It should be noted that TOPO has already been used in the synthesis of $CsPbX_3$ NCs. However, it was employed either in combination with primary amines[25] or in combination with octylphosphonic acid,[26] but in the latter case the role of TOPO in the synthesis has not been investigated. Using the approach reported in this work, we are able to synthesize bright, size-tunable $CsPbBr_3$ nanocubes, with narrow size distributions and in high yields (61 atom % in Pb), by varying the reaction temperature (in the range of 25−140 °C) and the [TOPO]/[OA] ratio. These two parameters, which influence the OA−TOPO acid−base equilibrium, regulate the solubility and reactivity of $PbBr_2$ and consequently the mean size and size distribution of the NCs. We carry out these reactions in air, thus not requiring degassing steps.

We investigate the growth of the NCs, their stability, and the relationship between their ligand shell and photoluminescence efficiency using ^1H and ^{31}P NMR, in combination with optical, X-ray, and computational techniques. We find that the ligand shell does not comprise any phosphine-containing compounds; rather, it is only made of Cs-oleate, which is dynamically bound to the surface. We also determine that an optimal surface coverage of Cs-oleate on the surface of our NCs allows us to achieve high photoluminescence quantum yields (PLQYs) up to 61%. Such an optimal coverage can be maintained throughout sequential washing with polar solvents (such as acetone), provided that additional OA is supplied during the procedure. The TOPO/OA route that is proposed here offers a number of advantages with respect to the standard oleylamine/OA route: it has reaction yields close to theoretical yields, it is free of layered perovskite impurities or nanosheet-/nanoplatelet-shaped NCs, and it delivers NCs with a simple ligand shell.

Finally, we show that the synthesis can be extended to other protic acids, such as *n*-tetradecylphosphonic acid and diisooctylphosphinic acid, allowing us to obtain NCs capped with different ligand shells.

EXPERIMENTAL SECTION

Materials. Trioctylphosphine oxide (99%, TOPO) was purchased from Strem Chemicals. *n*-Tetradecylphosphonic acid (TDPA) was purchased from PCI Synthesis. Acetone (99.5%), cesium carbonate (Cs_2CO_3, 99%), *N*,*N*-dimethylformamide (99.8%, anhydrous), dimethyl sulfoxide (99.9%), oleylamine (70%, OlAm), oleic acid (90%, OA), diisooctylphosphinic acid (90%, DOPA), 1-octadecene (90%), toluene (≥99.7%), toluene-d_8 (*d*-toluene, 99.8 atom % D), and $PbBr_2$ (≥98%) were purchased from Sigma-Aldrich. We used all chemicals without any further purification unless otherwise stated.

$PbBr_2$ (93 mM) solution in TOPO. TOPO (0.75 g, 1.93 mmol) and $PbBr_2$ (30 mg, 0.16 mmol) were heated to 75 °C on a hot plate with stirring. Once all the lead halide had reacted, the clear solution was cooled, forming a white solid.

Preparation of Cs Precursors. *Solution 1: Cs-Oleate (0.15 M) in 1-Octadecene.* Cs_2CO_3 (0.406 g, 1.25 mmol) and OA (1.7 mL, 5.39 mmol) were degassed in 15.0 mL of ODE in a three-neck round-bottomed flask under vacuum at 100 °C for 1 h followed by reacting under nitrogen at 140 °C. The colorless Cs-oleate solution was stored in a glovebox.

Solution 2: Cs-Oleate (0.15 M) in Oleic Acid. Cs_2CO_3 (0.122 g, 0.38 mmol) and OA (5.0 mL, 15.8 mmol) were degassed in a three-neck round-bottomed flask under vacuum at 100 °C for 1 h followed by reacting under nitrogen at 140 °C. The colorless Cs-oleate solution was stored in a glovebox.

Syntheses: General Considerations. Synthetic procedures were carried out in air unless otherwise stated. Cs precursors were stored in a glovebox, and reactions were performed in vials on a hot plate equipped with a thermocouple and a magnetic stirrer at 800 rpm.

Synthesis of Cube-Shaped $CsPbBr_3$ Nanocrystals (NCs). In a typical synthesis, $PbBr_2$ (60 mg, 0.16 mmol), TOPO (1.0 g, 0.88 g/mL, 2.59 mmol), and OA (400 μL, 1.27 mmol) were heated to 100 °C in ODE (5.0 mL), providing a clear solution. The temperature was set to the desired reaction temperature (25−140 °C), and Cs-oleate was injected (1.0 mL of solution 2, preheated to the same temperature). After 30 s of growth, the vial was plunged into an ice bath to quench the reaction. To separate the NCs, we centrifuged them in the absence of an antisolvent and redispersed them in toluene. Parameters of optimization experiments are given in Table S1 of the Supporting Information.

Washing of NCs. To wash the NC dispersion, we used acetone, at a volume ratio of 2:1. We centrifuged at 3000 rpm for 5 min, discarded the supernatant, and redispersed the NCs in toluene. For the best results, we added 5 μL of oleic acid per 1 mL of NCs upon redispersion. We repeated this process a second time to obtain washed NCs.

Inductively Coupled Plasma−Optical Emission Spectroscopy (ICP-OES). We determined the concentration of NC dispersions in Pb by ICP-OES on an aiCAP 6000 spectrometer (Thermo Scientific). We used aqua regia to digest the NC solution overnight prior to the measurements.

Dynamic Light Scattering (DLS) Measurements. The hydrodynamic diameter of the NCs was determined by DLS measurements on a Malvern Zetasizer (Nano Series, Nano ZS) instrument. The scattered intensity was collected at a 173° backscattered geometry with a 633 nm laser source. For each sample, three measurements were taken with 10−20 acquisitions.

Nuclear Magnetic Resonance. We used a Bruker Avance III 400 MHz spectrometer, equipped with a broad band inverse probe (BBI), to investigate the acid−base interactions of TOPO. To perform NMR studies on the NCs, we used a Bruker DRX400 spectrometer (400.13 MHz) equipped with a Bruker 5 mm BBI Z-gradient probe head, affording a maximum gradient strength of 53.5 G/cm.

After an automatic 90° calculation on each sample tube, ^1H NMR spectra were accumulated, at 300 K, as follows: 1 transient and 64K data points, no steady state scans, over a spectral width of 20.55 ppm (offset at 6.18 ppm), at a fixed receiver gain (1).

Inverse Gated ^1H Decoupled ^{31}P NMR. Spectra were acquired, at 300 K, as follows: 1 transient and 64K data points, no steady scans, over a spectral width of 200.45 ppm, (offset at 0.00 ppm), at a fixed receiver gain (1820).

NMR Spectra at Different Temperatures (288−354 K). We actively monitored the temperature, and the samples were left to equilibrate for at least 5 min inside the probe before the acquisition. The ^1H NMR spectra were measured with 4 transients and an interpulse delay of 30 s, while the ^{31}P spectra were measured with 1 transient and an interpulse delay of 60 s.

We referenced all NMR chemical shifts to a 0.049 M TMS (tetramethylsilane) internal reference solution, at 0.0 ppm for ^1H, and to a TEP (triethyl phosphate) 0.049 M external reference solution, at 0.0 ppm for ^{31}P.

2D Diffusion Ordered Spectroscopy (DOSY). Experiments were acquired at 297 K using a ledbp pulse sequence (ledbpgp2s of the Bruker library),[27] with a diffusion time (Δ) of 300 ms and a total gradient pulse duration (δ) of 4 ms. The gradient strength (G) was linearly incremented in 32 steps from 5 to 95% of its maximum value. The following equation describes the intensity decay:

$$\ln \frac{I}{I_0} = -(\gamma\delta)^2 D_t \left(\Delta - \frac{\delta}{3} - \frac{\tau}{2}\right) G^2$$

DOI: 10.1021/jacs.8b08978
J. Am. Chem. Soc. 2018, 140, 14878−14886

in which I is the observed intensity, I_0 is the nonattenuated signal intensity, D_t is the diffusion translational coefficient, γ is the gyromagnetic ratio of ^{1}H, and τ is the time between bipolar gradients. We obtained diffusion coefficients by analyzing the signal intensity decay as a function of the gradient strength G of at least three different resonances by using a least-squares linear fitting.

2D Nuclear Overhauser Effect Spectroscopy (^{1}H–^{1}H NOESY). Experiments (noesygpph of the Bruker library)[28] were performed with a mixing time of 300 ms and 2048 data points in the direct dimension for 256 data points in the indirect dimension, accumulating 32 transients each.

We referenced the chemical shifts of the DOSY and NOESY NMR spectra to the nondeuterated residual peak of *d*-toluene at 7.09 ppm.

Steady-State UV–Vis Extinction Spectroscopy, Steady-State Photoluminescence Spectroscopy, and Photoluminescence Quantum Yields. We recorded optical extinction and photoluminescence spectra of toluene dispersions in quartz cuvettes with a 1 cm path length, employing a Varian Cary 300 UV–vis spectrophotometer and a Varian Cary Eclipse fluorescence spectrophotometer, respectively. We measured absolute photoluminescence quantum yields using an Edinburgh Instruments FLS920 spectrofluorometer equipped with an integrating sphere, and the optical density of the NC solution was 0.1 at 420 nm.

Transmission Electron Microscopy (TEM). NC dispersions were drop-cast on carbon-coated 200 mesh copper grids. We acquired bright field TEM images on a JEOL JEM-1011 microscope (W filament) operating at an accelerating voltage of 100 kV.

X-ray Diffraction (XRD). Concentrated NC dispersions are drop-cast onto a zero diffraction silicon substrate. We conduct XRD measurements on a PANalytical Empyrean X-ray diffractometer equipped with a 1.8 kW Cu Kα ceramic X-ray tube and PIXcel3D 2 × 2 area detector, operating at 45 kV and 40 mA.

X-ray Photoelectron Spectroscopy. This was performed on a Kratos Axis Ultra^{DLD} spectrometer, equipped with a monochromatic Al Kα source, which was operated at 20 mA and 15 kV. Concentrated solutions of NCs were drop-cast onto freshly cleaved highly oriented pyrolytic graphite substrates. Survey scans were carried out using an analysis area of 300 × 700 μm and a pass energy of 160 eV. High-resolution scans were performed on the same analysis area, but with a pass energy of 10 eV. The Kratos charge neutralizer system was used on all specimens. Spectra were charge corrected to the main line of the carbon 1s spectrum (adventitious carbon) set to 284.8 eV. Spectra were analyzed using CasaXPS software (version 2.3.17).

Computational Methods. A model of a $CsPbBr_3$ nanocube with an edge length of 2.4 nm was built by cleaving a cubic bulk structure along the (100) planes. The NC is terminated with a layer of CsBr ions, and the charge balance was obtained by removing excess Cs from the surface. Under such conditions, after geometry relaxation, we obtained an effective trap-free and orthorhombic NC as demonstrated previously.[13,29] Several types of surface termination and passivation were employed (vide infra), and all structures were optimized under vacuum at the density functional theory (DFT) level of theory using the PBE exchange-correlation functional[30] and a double ζ basis set plus polarization functions.[31] We accounted for scalar relativistic effects by employing effective core potential functions in the basis set. Spin–orbit coupling effects were not included in the calculations. All calculations were performed using the CP2K quantum chemical package.[32]

RESULTS AND DISCUSSION

OA–TOPO Acid–Base Equilibrium in the Solubility of $PbBr_2$. First we note that TOPO is able to solubilize $PbBr_2$ in the absence of a solvent, forming a clear TOPO–$PbBr_2$ solution above 50 °C. This solution solidifies to a white solid upon cooling, matching with the melting point of TOPO (ca. 50 °C). The resulting product fluoresces orange under ultraviolet excitation, which is similar to the case for lead bromide dissolved in DMSO and DMF (Figure 1). From this, we infer that TOPO complexes $PbBr_2$ in a way similar to that for carbonyl and thionyl groups.[33] We examine the interaction of TOPO with $PbBr_2$ by ^{31}P NMR in dilute toluene solutions. As shown in Figure 1b, the ^{31}P signal of TOPO is shifted downfield in the presence of $PbBr_2$ (24:1 mole ratio), and this is attributed to an interaction of the oxygen atom of TOPO with $PbBr_2$.[34] The addition of oleic acid (OA) to dilute TOPO–$PbBr_2$ solutions leads to the precipitation of solid $PbBr_2$ (see Figure S1 of the Supporting Information), indicating a competing interaction between the protic acid (OA) and $PbBr_2$ for the oxygen of TOPO.

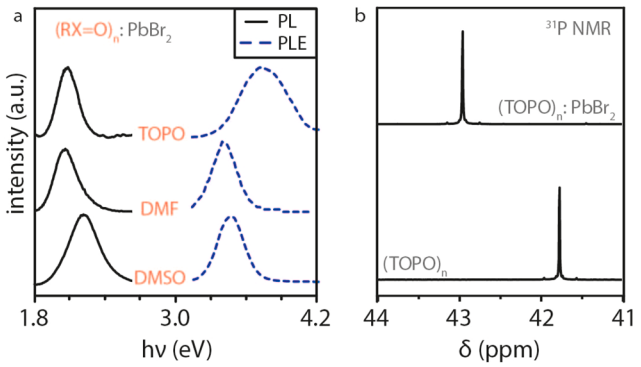

Figure 1. (a) Photoluminescence (PL, solid line) and photoluminescence excitation (PLE, dashed line) spectra of TOPO and dimethyl sulfoxide (DMSO) and dimethylformamide (DMF) solutions of $PbBr_2$ ([$PbBr_2$] = 93 mM in the TOPO solution and [$PbBr_2$] ≤ 50 mM for DMSO and DMF solutions). (b) ^{31}P NMR spectra of TOPO and TOPO–$PbBr_2$ in *d*-toluene ([TOPO] = 0.81 M, [$PbBr_2$] = 0.03 M).

We then employ ^{1}H and ^{31}P NMR in order to study the acid–base interaction between OA and TOPO in *d*-toluene (see Figure 2). In the presence of TOPO, the α-CH_2 resonances of OA shift downfield (Figure 2a and Figure S2), which we attribute to hydrogen bonding of OA with TOPO, in analogy with a previous work of ours on acid–base equilibria between OA and oleylamine.[12] Over the same range of acid:base ratios (see Table 1), a 10-fold larger downfield shift is observed for the narrow ^{31}P signal of TOPO as a result of hydrogen bonding/protonation of TOPO (Figure 2b), which is in agreement with previous studies.[35] The greater shift that is observed with respect to the ^{1}H signal is due to the contribution of paramagnetic shielding to the chemical shift, which is the dominant term for the ^{31}P nuclide (and in general for hetero nuclei) and is absent for the ^{1}H nuclide.[36]

The ^{31}P signal is therefore a powerful probe with regard to investigating acid–base equilibria between OA and TOPO. This was particularly evident when we recorded the ^{1}H and ^{31}P NMR spectra as a function of the temperature. While heating of a TOPO–OA (1:1 molar ratio) solution from 15 to 75 °C only causes a marginal shift to the α-CH_2 resonances of OA (see Figure S3), the ^{31}P signal of TOPO visibly shifts upfield (Figure 2c, red squares). Note that, even in a solution containing TOPO alone, the ^{31}P signal shifts upfield when the temperature is increased (Figure 2c, black squares), but to a lesser extent than in a TOPO–OA mixture. We attribute the greater upfield shift of the ^{31}P signal in the TOPO–OA mixture at higher temperatures to the deprotonation of TOPO-H$^+$. This is in line with the fact that an acid–base reaction is exothermic, therefore increasing the temperature shifts the equilibrium toward the neutral forms of acid (OA) and base (TOPO).

DOI: 10.1021/jacs.8b08978
J. Am. Chem. Soc. 2018, 140, 14878–14886

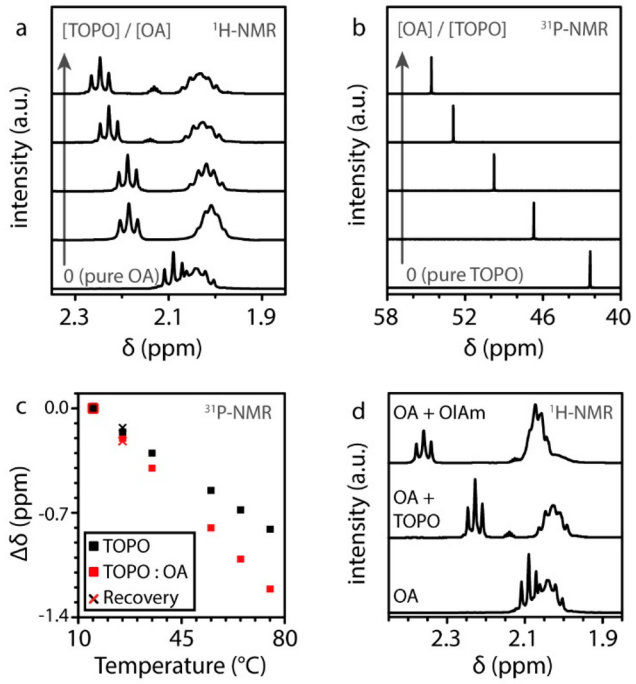

Figure 2. Selected regions from the (a) ^{1}H and (b) ^{31}P NMR spectra of *d*-toluene solutions containing mixtures of TOPO and OA. The molar ratios of TOPO to OA ratios are varied from 1:0.5 to 1:4 (see Table 1 for further details) (c) Temperature dependence of the ^{31}P NMR signal of *d*-toluene solutions of TOPO (black) and TOPO−OA (red, 1:1 molar ratio). (d) ^{1}H NMR spectra of *d*-toluene solutions of OA, TOPO−OA and oleylamine (OlAm)−OA at the same concentrations (0.43 M) of acid and base.

Table 1. TOPO−OA Solutions in *d*-Toluene Investigated with ^{1}H and ^{31}P NMR[a]

TOPO, M	OA, M	[TOPO]:[OA]
0.43	0	1:0
0.43	0.22	1:0.5
0.43	0.43	1:1
0.43	0.86	1:2
0.43	1.72	1:4
0	0.86	0:2

[a]See Figure 2.

The effects of temperature and concentration of OA on the acid−base equilibrium are used in our syntheses to modulate the reactivity of $PbBr_2$ in the TOPO−OA mixture, as will be described later in detail. Furthermore, it should be noted that, in comparison to oleylamine, we find that TOPO induces a smaller (downfield) shift to the α-CH_2 resonances of oleic acid at equimolar concentrations (Figure 2d). This is in agreement with previous reports showing that the proton affinities of RX═O bases are lower than those of amines.[37]

Synthesis of $CsPbBr_3$ NCs in the OA/TOPO Mixture. We take advantage of this acid−base interaction between TOPO and OA to synthesize $CsPbBr_3$ nanocubes via an injection route.[38] In short, we prepare a solution containing the Cs precursor (Cs-oleate) by reacting Cs-carbonate with OA (to achieve low/high concentrations of OA, ODE/OA was used as solvent). We inject the Cs-oleate solution (1−2 mL, 0.0.75−0.40 M) into an 1-octadecene (ODE) solution containing TOPO (1.0 g, 0.88 g/mL, 0.40 M), oleic acid (0.24 M), and $PbBr_2$ (60 mg, 25 mM). We adjust the volume of ODE in each experiment in order to fix the volume of the ODE solution (6.5 mL) as well as the concentrations of TOPO and $PbBr_2$. We report the details in the Experimental Section and in the Supporting Information. Upon injection, the initially colorless Pb solution turns immediately colored (green or yellow, depending on the temperature and NC size), indicating the formation of $CsPbBr_3$. The overall reaction can be described by the equation

$$2Cs^+ + 3PbBr_2 \rightarrow 2CsPbBr_3 + Pb^{2+}$$

which allows a maximum conversion of $PbBr_2$ into $CsPbBr_3$ of 2/3 in terms of Pb. After 30 s, we quench the reaction in an ice bath and separate the NCs from the reaction mixture by centrifugation. We do this in the absence of an antisolvent, and we redisperse the NCs in toluene; henceforth, these will be referred to as "as-synthesized NCs".

We perform a series of syntheses at a constant temperature (75 °C) and growth time (30 s) but varying the total [OA], to elucidate the role of the acidity of the medium in the NC synthesis. As shown in Figure 3a, the average NC size

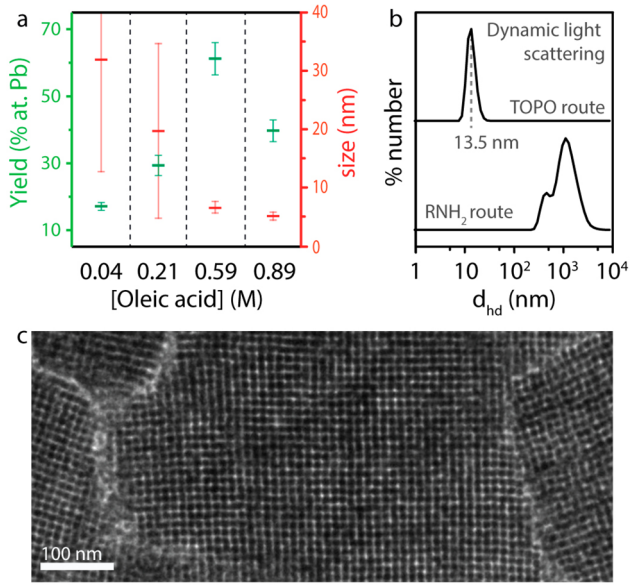

Figure 3. (a) Reaction yield (atom % Pb) and particle mean size and size distribution (the latter indicated by the red error bars) of samples synthesized with various concentrations of OA under otherwise fixed reaction conditions (a reaction temperature of 75 °C, a growth time of 30 s, and fixed concentrations of TOPO and $PbBr_2$; the concentration of OA is the total concentration in the reaction mixture after the injection of the Cs-oleate precursor). (b) (top) Dynamic light scattering (DLS) measurement of an as-synthesized toluene dispersion of 6 nm NCs with an optical density of 3 at 2.42 eV (d_{hd} is the hydrodynamic radius). (bottom) DLS of a dispersion of NCs of similar size, optical density, and age prepared via the amine route.[12] (c) TEM image of a 3D superstructure of $CsPbBr_3$ NCs.

decreases (from 32.1 to 5.3 nm) and the size distribution narrows quite remarkably (19.3 nm/60% to 0.8 nm/15%) as the [OA] used in the synthesis is increased from 0.04 M up to 0.89 M. Concomitantly, the reaction yield in Pb increases from 17 to 61% (as determined by an ICP analysis of as-synthesized samples). Our results show that we can synthesize monodisperse $CsPbBr_3$ NCs in yields that are close to the theoretical limit. In this case, due to a slight deficiency in Cs, the

DOI: 10.1021/jacs.8b08978
J. Am. Chem. Soc. 2018, 140, 14878−14886

theoretical yield in terms of Pb is actually stoichiometrically limited to 62.5%. The reaction yield at the highest acid concentration is likely underestimated, since a portion of the particles are lost during the separation process due to their reduced dimensions (<5 nm), and this is reflected in Figure 3a.

Combining the observations regarding NC size and reaction yield allows us to conclude that the acid destabilization of the $PbBr_2$ solution controls both the reactivity of $PbBr_2$ and the extent of nucleation. We find that balancing the total amount of acid (OA) between the Cs and $PbBr_2$ solutions is important, as the absence of OA in the starting Pb solution results in larger sizes and broader size distributions (Figure S4). Note that the concentration of OA, [OA], in the ODE−TOPO−$PbBr_2$ solution is limited by the reprecipitation of $PbBr_2$, as shown earlier. Finally, we observe little or no size variation over the course of 10 min of growth time (see Figure S5 for an aliquot study). The absence of size defocusing/Ostwald ripening in this reacting scheme is quite unusual and will be discussed later.

A DLS analysis on a concentrated toluene dispersion of 6 nm $CsPbBr_3$ NCs shows a single narrow peak at ca. 13.5 nm (Figure 3b). This value is in line with the diameter of a sphere containing one nanocube capped with a monolayer of ligands, and it shows that the particles are dispersed evenly. Note that NCs of comparable size, size distribution, and age, synthesized via the oleylamine−OA route employing low [OA] (optimized for a narrow size distribution), tend to aggregate and lose colloidal stability, as is shown in Figure 3b (see Figure S6 for additional details on the synthesis of this latter sample). Also, a more thorough comparison of the TOPO−OA route with the oleylamine−OA route can be found in the last section of this work. We further attest to the monodispersity of the NCs that are prepared via the TOPO route by their tendency to form three-dimensional cubic superstructures with coherence lengths of hundreds of nanometers when they are drop-cast on TEM grids from concentrated dispersions (see Figure 3c).

We then carry out a series of experiments in which we tailor the temperature of the reaction to tune the NC size (see Figure 4). Under otherwise identical conditions, we are able to isolate NCs with edge lengths of 11, 6, and 3 nm by conducting the syntheses at 140, 50, and 25 °C, respectively. While the $CsPbBr_3$ NCs that were synthesized between 140 and 50 °C typically exhibit narrow size distributions (σ = 10%), sharp absorption onsets, clear excitonic peaks, and a green PL that is characterized by narrow PL full widths at half-maximum (70−80 meV), the NCs prepared at room temperature exhibit a blue emission but with broader optical features. Note that the 3 nm NCs are in the strong confinement regime (λ_{PL} = 2.65 eV), where small size variations lead to strong changes in the electronic structure.[3,39,40] Furthermore, their isolation is challenging and requires the use of copious amounts of polar solvents, such as acetone, which likely causes the NCs to degrade slightly.

Also, in the same way that excess amine was found to be detrimental to $CsPbBr_3$ NCs,[12,23,24] excess TOPO can also drive the transformation of $CsPbBr_3$ to Cs_4PbBr_6 NCs. This occurs through a dissolution and recrystallization process similar to that for the amine case,[24] as is discussed in sections S7 and S8 in the Supporting Information. The subsequent addition of acid reverses the phase change, but not the crystal dimensions, and we therefore denote it as quasi-reversible.

The final synthesis parameter we investigate is the concentration of Cs-oleate that we inject ($[Cs\text{-oleate}]_I$, I stands for injected). As we increase $[Cs\text{-oleate}]_I$ from 0.10 to 0.30 M, the photoluminescence quantum yield (PLQY) of as-synthesized NC dispersions increases from 18 to 61% (see Figure 5a). Upon a further increase to 0.4 M, we observe a decrease in the PLQY to 43%. As we show in Figure S9, there is negligible change in the NC size over this range of $[Cs\text{-oleate}]_I$; therefore, we attribute the variations in PLQY to a change in surface passivation.

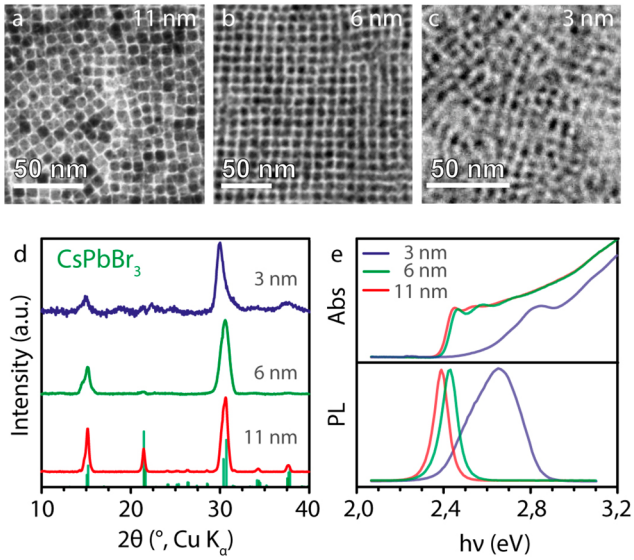

Figure 4. (a−c) TEM images, (d) XRD patterns (reference: COD 4510745), and (e) absorbance and photoluminescence (PL) spectra of $CsPbBr_3$ NCs synthesized with TOPO at reaction temperatures of 25 (3 nm), 50 (6 nm, σ = 10%), and 140 °C (11 nm, σ = 10%).

Surface Chemistry of the $CsPbBr_3$ NCs. We perform a series of analyses and calculations which, overall, strongly indicate that the surface of our NCs is passivated by Cs-oleate and that TOPO is essentially absent from the ligand shell. First, we note that $CsPbBr_3$ nanocubes, as well as LHP nanocubes in general, are terminated by (100) facets comprised of either a $PbBr_2$ or a CsBr plane. We use X-ray photoelectron spectroscopy (XPS) to reveal that all four samples in this investigation ($[Cs\text{-oleate}]_I$ = 0.1, 0.2, 0.3, 0.4 M) exhibit Br:Pb ratios in the range of 2.3−2.5. These numbers are in good agreement with the expected value of ~2.7 for $PbBr_2$-terminated NCs of this size, passivated with a shell of Cs^+ and a mixture of bromide, oleate, and other anionic species. We also see that, with increasing $[Cs\text{-oleate}]_I$, the Cs:Pb ratio increases and the Br:Cs ratio decreases (see Figure 5b), confirming that the NC surface becomes richer in Cs as $[Cs\text{-oleate}]_I$ is increased.

Typically, LHP NCs are passivated by pairs of X-type ligands, also named X_2 ligands in Green's covalent bond classification scheme,[41] such as alkylammonium halides, carboxylates, etc.[22] Here, according to XPS measurements, no phosphorus is observed in strongly emitting washed samples (i.e., $P/Pb_{surface} \leq 2$ atom %),[42] suggesting that Cs-oleate is the only compound passivating the NCs. To further support this idea, we use DFT to compute the adsorption energies of the different ligands that, according to our reaction scheme, could possibly be passivating these NCs: namely, Cs-oleate, OA, and the acid−base salts of TOPO with OA and HBr. To facilitate the calculations, we reduce the lengths of the aliphatic chains to one carbon (e.g., acetic acid is used instead

DOI: 10.1021/jacs.8b08978
J. Am. Chem. Soc. 2018, 140, 14878−14886

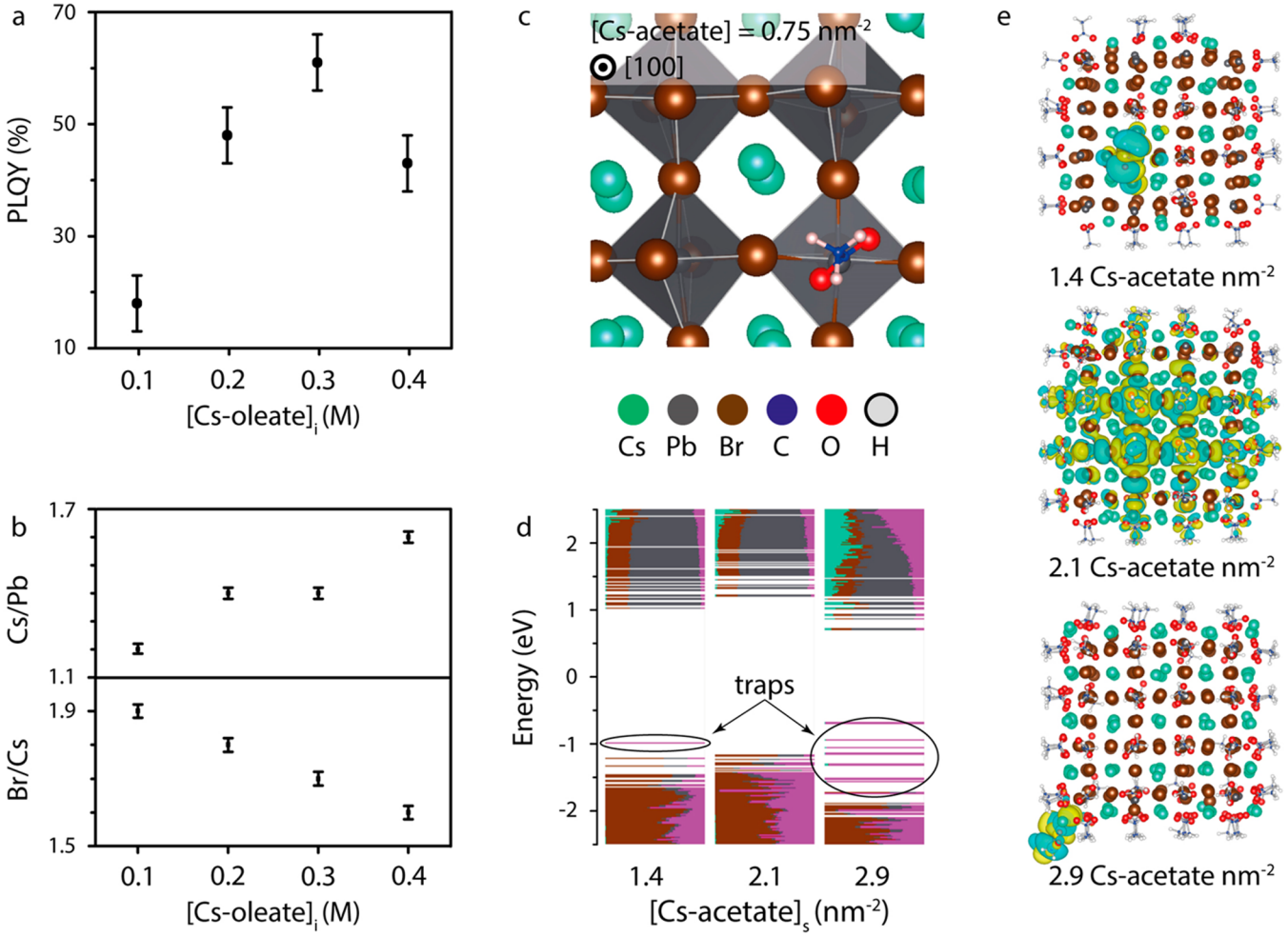

Figure 5. (a) PLQY and (b) Cs:Pb and Br:Cs ratios (as determined by XPS) of a series of $CsPbBr_3$ NCs synthesized by varying the concentration of Cs-oleate in the injection solution, $[Cs\text{-oleate}]_I$. (c) Relaxed structure, computed at the DFT/PBE level of theory, for a lead bromide terminated $CsPbBr_3$ (100) surface, passivated by CsBr and Cs-acetate. (d) Electronic structure of a $CsPbBr_3$ NC ($2.4 \times 2.4 \times 2.4$ nm^3) as a function of its surface coverage in Cs-acetate (denoted as $[Cs\text{-acetate}]_s$). The contribution of each atom type to a molecular orbital is given with a similar color code: green (Cs), gray (Pb), brown (Br), and purple (carboxylate ligand). The isosurface of the highest occupied molecular orbital (i.e., the valence band edge orbital) for each surface passivation is also shown in (e) with a counter value of 0.02 e/bohr^3. At low and high surface concentrations of Cs-acetate, surface traps appear as localized states. At intermediate concentrations (2.1 Cs-acetate nm^{-2}), the valence band edge state is delocalized and free of traps.

of oleic acid). We consider that each ligand moiety binds onto a $PbBr_2$-terminated (100) surface as a pair of charged species (e.g., acetic acid dissociating into oleate and proton) and a 2.4 nm nanocube is used as a model (additional details are discussed in the Supporting Information). The results show that the added ion pairs accommodate on the NC surface, filling the perovskite lattice sites, as illustrated in Figure 5c for Cs-acetate and in Figure S10 for $(CH_3)_3PO{-}HBr$. Negative (i.e., stabilizing) adsorption energies are found for all four ligand systems under investigation, and Cs-acetate is found to exhibit the highest affinity toward the NC surface, which is in agreement with the experiments (see section S10 of the Supporting Information for further details).

To explain the trend in PLQY, we also compute the NC electronic structure as a function of the surface coverage in Cs-acetate, denoted as [Cs-acetate] (Figure 5d,e). Here, each molecular orbital is decomposed and color-coded in terms of contributions of a given atom type. We note that the addition or removal of Cs-acetate ligands from an intermediate passivated trap-free NC with a surface ligand concentration of 2.1 ligands/nm^2, leads to the creation of in-gap trap states that could act as nonradiative recombination centers. Note that the appearance of traps occurs at very high or at very low surface concentrations of ligands, respectively (Figure 5d). This is in line with the trend that is found in the PLQY as a function of $[Cs\text{-oleate}]_I$ reported in Figure 5a.

To investigate the dynamics of the Cs-oleate capping layer, we perform ^{1}H NMR on NC dispersions in *d*-toluene. For this purpose, we wash the NCs twice with acetone. The OA resonances can be clearly identified but are broader and shifted with respect to those of free oleic acid (Figure 6a), indicating the presence of tightly bound oleate species, active dynamic processes, or both. We infer a confirmation of the interaction of oleate species with the NC surface by 2D ^{1}H NOESY (Figure 6b, top spectrum). First, a negative (red) NOE cross peak is observable in the NC sample, whereas positive NOE cross peaks are observed on free ligands (OA, Cs-oleate, see Figure S11.1). The negative cross peak is characteristic of species with long correlation times (τ_c) that move more slowly in solution in comparison to small free molecules. These

DOI: 10.1021/jacs.8b08978
J. Am. Chem. Soc. 2018, 140, 14878−14886

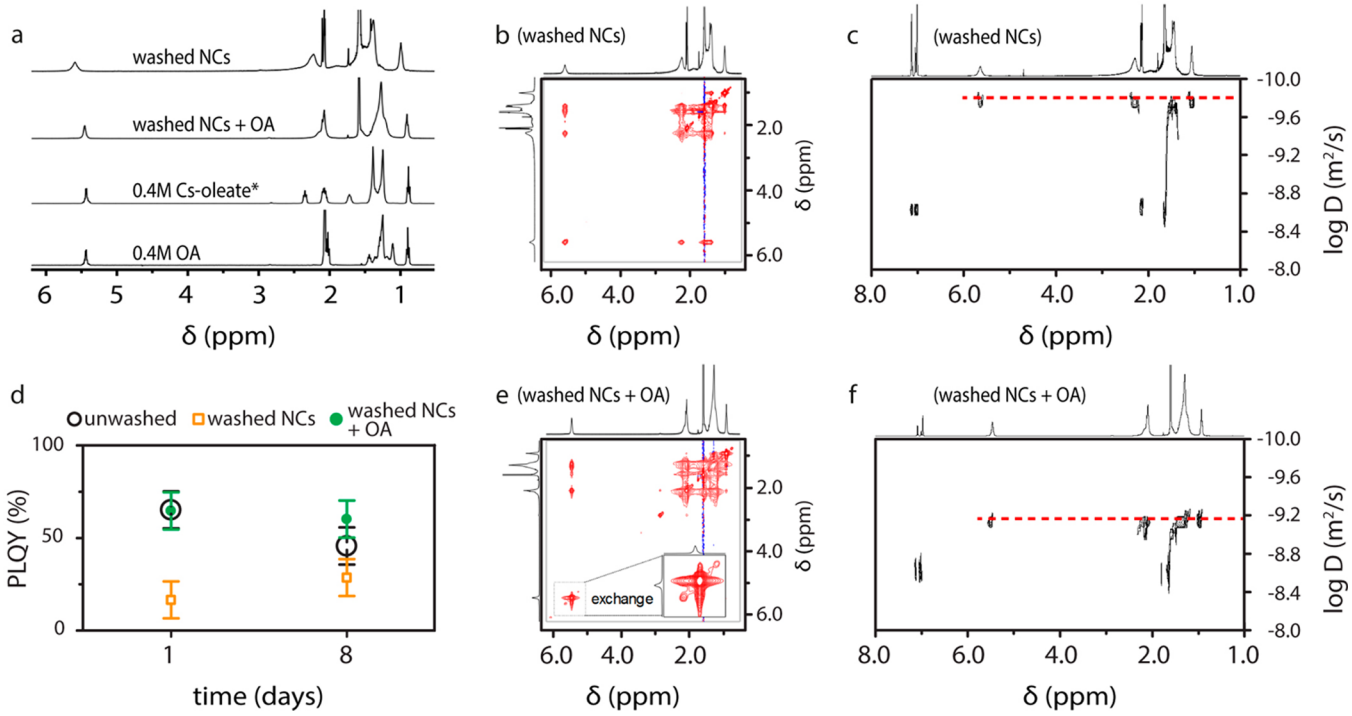

Figure 6. (a) ^{1}H NMR spectra of *d*-toluene solutions of oleic acid (OA), Cs-oleate (*$[OA]_{total}$ = 0.95 M), and dispersions containing $CsPbBr_3$ NCs washed with (i) acetone (washed NCs) and (ii) acetone with small amounts of OA added afterward (5 μL of OA per 1.0 mL of NC). The sample is named "washed NCs + OA". Further details regarding the washing procedures are described in the Experimental Section. (b) ^{1}H-NOESY and (c) ^{1}H-DOSY spectra of the "washed NCs" sample indicating the presence of surface-bound oleate species with an overall diffusion coefficient (D) of 242 $\mu m^2/s$. (d) PLQY of as-synthesized (unwashed) NCs, "washed NCs", and "washed NCs + OA" samples. The presence of residual amounts of OA allows maintenance of a PLQY of ca. 60% in the "washed NCs + OA" sample for over 1 week. (e) ^{1}H-NOESY and (f) ^{1}H-DOSY spectra of the "washed NCs + OA" sample (D = 624 $\mu m^2/s$) revealing the rapid exchange mechanism between surface-bound oleate and free oleic acid.

findings are supported by diffusion ordered spectroscopy (DOSY, Figure 6c), where a diffusion coefficient of 242 $\mu m^2/s$ is found, which is considerably smaller than that of free oleic acid or Cs-oleate in *d*-toluene (725 and 726 $\mu m^2/s$, respectively, 0.2 M solutions, Figure S11.2). From this, we calculate the bound fraction of oleate species to be ca. 76% following the method of de Roo et al.[22]

At this point, we note that the washing process causes a drop in the PLQY of our NCs. However, we can maintain PLQYs of over 60% by adding small amounts of OA (0.5 vol % per mL of NCs) after each washing/redispersion cycle (Figure 6d). This suggests that the presence of free oleic acid can prevent the desorption of bound Cs-oleate and can therefore maintain high PLQY values. In the ^{1}H spectrum of this sample (Figure 6a, second spectrum from the top), we observe two partially overlapped broad peaks in the double-bond region which we attribute to bound oleates (5.60 ppm, very weak signal but visible in Figure S11.3) and to free OA (5.46 ppm), respectively. The free OA signal exhibits a line broadening that is indicative of exchange processes, and this is confirmed by the cross peak between the two double-bond signals in a 2D ^{1}H NOESY experiment (Figure 6e, inset), along with negative NOE cross peaks. The ^{1}H DOSY experiment (Figure 6f), instead, shows a considerable increase in the weighted average diffusion coefficient (624 $\mu m^2/s$) of the free and bound states, tending to the value of free OA. Such evidence is in line with a rapid exchange mechanism.[43]

We also perform DLS measurements on our as-synthesized and washed (with added OA) NCs to monitor their colloidal stability alongside their PLQY stability. We find that there is no difference in the as-synthesized sample over the 8 day period, but we do see an indication of aggregation in the washed sample (Figure S12).

Comparison with the Oleylamine/OA Route and Extension to Other Acids. In a previous paper from our group, we investigated how acid−base interactions control the morphology of $CsPbBr_3$ NCs synthesized via the amine route.[12] In that work, we demonstrated that high acidity levels promote the formation of two-dimensional structures and that, in order to narrow the size dispersion of $CsPbBr_3$ nanocubes, the concentration of acid and base should be kept to a minimum. Here, using TOPO to solvate $PbBr_2$, we show that two-dimensional NCs are not formed at high acidity levels and that high acidity levels are actually key to obtaining monodisperse $CsPbBr_3$ nanocubes at reaction yields close to the theoretical yields.

We further demonstrate this point by expanding this synthesis to different acids: namely, diisooctylphosphinic acid (DOPA) and *n*-tetradecylphosphonic acid (TDPA). First we determine the affinity of the different acids toward TOPO using ^{31}P NMR (TDPA > OA > DOPA) and then run the synthesis of $CsPbBr_3$ NCs with each of the three acids under equimolar conditions. As shown in Figure S13, TDPA, which exhibits the strongest affinity toward TOPO, yields nearly monodisperse nanocubes (10 nm, σ = 10%), similar to those obtained with OA. However, DOPA, which has the weakest affinity toward TOPO, produces larger and more polydisperse NCs (57 nm, σ = 35%). Nevertheless, by increasing the concentration of DOPA in the synthesis, smaller NCs with narrower size distributions can be obtained (7 nm, σ = 28%).

DOI: 10.1021/jacs.8b08978
J. Am. Chem. Soc. 2018, 140, 14878−14886

These results are in line with previous studies observing that acidic environments increase the crystallization rate of millimeter-sized LHP crystals in carbonyl and thionyl dipolar solvents.[10]

For further comparison with the oleylamine route, we have prepared two batches of ca. 6 nm nanocubes with similar size distribution (σ = 10%). While we obtain NCs synthesized via the TOPO route at a reaction yield in Pb of ca. 60 atom %, we obtain the NCs synthesized via the oleylamine route in a reaction yield of ca. 8%. Also, the NCs synthesized via the amine route aggregate and quickly lose colloidal stability, as discussed earlier (Figure 3b). We attribute the low reaction yields and poor colloidal stability of these NCs to the low amount of acid used in their preparation. Although a low amount of acid is required to avoid the coformation of two-dimensional nanostructures and to improve the size dispersion of the nanocubes,[12] it is too low to efficiently destabilize the starting lead complexes and to counter the desorption of surface-bound oleate species which, in turn, likely lead to NC aggregation.

Similarly to the amine route, the passivation of the NCs synthesized in this work is carried out by pairs of X ligands (Cs-oleate), which tend to desorb and are in rapid exchange with free ligands.[22] However, the absence of an alkylammonium cation (e.g., oleylammonium) and the poor affinity of phosphine oxide ligands toward the NC surface allow us to obtain NCs passivated with a simpler ligand shell comprised of only one type of ligand.

A final note is on the absence of Ostwald ripening effect in our syntheses. Under the usually strong acidic conditions at which our syntheses are carried out, all TOPO molecules are hydrogen-bonded; hence, they are unable to stabilize any $PbBr_2$ species that would most likely be extracted from the NCs in the case of Ostwald ripening. This is different from the standard syntheses of nanocubes, in the presence of primary amines, in which strongly acidic environments are carefully avoided, forcing the synthesis to be conducted in an acid−base regime (low [acid], high [primary amine]) propitious to the extraction of $PbBr_2$.[12] On the other hand, when strongly acidic conditions are employed in the amine route, they lead to nanosheets/nanoplatelets with narrow thickness distributions, which might again suggest that Ostwald ripening also does not occur in this case.

CONCLUSION

In this work, we have demonstrated a new method for synthesizing LHP NCs in which we use TOPO to dissolve the lead halide precursor. We have highlighted several advantages that this new procedure has over the traditional amine route. In particular, we have demonstrated that it is possible to obtain monodisperse nanocubes in yields close to theoretical yields, which is of great interest for industrial applications. Furthermore, it is possible to extend the scope of our results to the synthesis of LHP thin films and single crystals based on polar carbonyl and thionyl molecules.

ASSOCIATED CONTENT

Supporting Information

The Supporting Information is available free of charge on the ACS Publications website at DOI: 10.1021/jacs.8b08978.

Synthetic details, control experiments on the synthesis of $CsPbBr_3$ via the TOPO−OA route, synthesis of Cs_4PbBr_6 NCs via the TOPO−OA route, quasi-reversible transformation of $CsPbBr_3$ NCs into Cs_4PbBr_6 NCs with TOPO−OA, synthesis of $CsPbBr_3$ via the primary amine route, additional and supporting NMR experiments, and further computational details (PDF)

AUTHOR INFORMATION

Corresponding Author

*E-mail for L.M.: liberato.manna@iit.it.

ORCID

Olivia J. Ashton: 0000-0002-0886-2110
Ivan Infante: 0000-0003-3467-9376
Henry J. Snaith: 0000-0001-8511-790X
Liberato Manna: 0000-0003-4386-7985

Present Address

[&]N.M.: Department of Chemistry of the SRM University-AP, Amaravati, Neerukonda, Guntur(Dt), Andhra Pradesh, India 522502.

Author Contributions

[▽]G.A. and O.J.A. contributed equally to this paper.

Notes

The authors declare no competing financial interest.

ACKNOWLEDGMENTS

O.J.A. extends thanks to their funding sources: the CDT in New and Sustainable Photovoltaics (EPSRC, EP/L01551X/1), Oxford Photovoltaics Ltd., and the Radcliffe Scholarship from University College, Oxford. I.I. acknowledges The Netherlands Organization of Scientific Research (NWO) for financial support through the Innovational Research Incentive (Vidi) Scheme (Grant No. 723.013.002). G.A., Q.A.A., and L.M. acknowledge the European Union seventh Framework Programme under Grant Agreement No. 614897 (ERC Consolidator Grant "TRANS-NANO"). The authors acknowledge Lea Pasquale, Filippo Drago, Giammarino Pugliese, Dr. Dmitry Baranov, and Dr. Vincenzo Caligiuri for their kind help with many of the measurements and Emma de Cecco for proofreading the manuscript. The computational work was carried out at CINECA Italy and on the Dutch national e-infrastructure with the support of the SURF Cooperative.

REFERENCES

(1) Kojima, A.; Teshima, K.; Shirai, Y.; M, T. *J. Am. Chem. Soc.* **2009**, *131*, 6050−6051.

(2) Yang, W. S.; Park, B.-W.; Jung, E. H.; Jeon, N. J.; Kim, Y. C.; Lee, D. U.; Shin, S. S.; Seo, J.; Kim, E. K.; Noh, J. H.; Seok, S. Il *Science* **2017**, *356*, 1376−1379.

(3) Protesescu, L.; Yakunin, S.; Bodnarchuk, M. I.; Krieg, F.; Caputo, R.; Hendon, C. H.; Yang, R. X.; Walsh, A.; Kovalenko, M. V. *Nano Lett.* **2015**, *15*, 3692−3696.

(4) Sutherland, B. R.; Sargent, E. H. *Nat. Photonics* **2016**, *10*, 295−302.

(5) Lee, S.; Park, J. H.; Nam, Y. S.; Lee, B. R.; Zhao, B.; Di Nuzzo, D.; Jung, E. D.; Jeon, H.; Kim, J.-Y.; Jeong, H. Y.; Friend, R. H.; Song, M. H. *ACS Nano* **2018**, *12*, 3417−3423.

(6) Jeon, N. J.; Noh, J. H.; Kim, Y. C.; Yang, W. S.; Ryu, S.; Seok, S. Il. *Nat. Mater.* **2014**, *13*, 897.

(7) Li, X.; Ibrahim Dar, M.; Yi, C.; Luo, J.; Tschumi, M.; Zakeeruddin, S. M.; Nazeeruddin, M. K.; Han, H.; Grätzel, M. *Nat. Chem.* **2015**, *7*, 703−711.

(8) McMeekin, D. P.; Sadoughi, G.; Rehman, W.; Eperon, G. E.; Saliba, M.; Hörantner, M. T.; Haghighirad, A.; Sakai, N.; Korte, L.;

DOI: 10.1021/jacs.8b08978
J. Am. Chem. Soc. 2018, 140, 14878−14886

Rech, B.; Johnston, M. B.; Herz, L. M.; Snaith, H. J. *Science* **2016**, *351*, 151−155.
(9) Swarnkar, A.; Marshall, A. R.; Sanehira, E. M.; Chernomordik, B. D.; Moore, D. T.; Christians, J. A.; Chakrabarti, T.; Luther, J. M. *Science* **2016**, *354*, 92−95.
(10) Nayak, P. K.; Moore, D. T.; Wenger, B.; Nayak, S.; Haghighirad, A. A.; Fineberg, A.; Noel, N. K.; Reid, O. G.; Rumbles, G.; Kukura, P.; Vincent, K. A.; Snaith, H. J. *Nat. Commun.* **2016**, *7*, 13303.
(11) Koscher, B. A.; Swabeck, J. K.; Bronstein, N. D.; Alivisatos, A. P. *J. Am. Chem. Soc.* **2017**, *139*, 6566−6569.
(12) Almeida, G.; Goldoni, L.; Akkerman, Q. A.; Dang, Z.; Khan, A. H.; Marras, S.; Moreels, I.; Manna, L. *ACS Nano* **2018**, *12*, 1704−1711.
(13) Krieg, F.; Ochsenbein, S. T.; Yakunin, S.; Ten Brinck, S.; Aellen, P.; Süess, A.; Clerc, B.; Guggisberg, D.; Nazarenko, O.; Shynkarenko, Y.; Kumar, S.; Shih, C. J.; Infante, I.; Kovalenko, M. V. *ACS Energy Lett.* **2018**, *3*, 641−646.
(14) Era, M.; Morimoto, S.; Tsutsui, T.; Saito, S. *Appl. Phys. Lett.* **1994**, *65*, 676−678.
(15) Tan, Z.-K.; Moghaddam, R. S.; Lai, M. L.; Docampo, P.; Higler, R.; Deschler, F.; Price, M.; Sadhanala, A.; Pazos, L. M.; Credgington, D.; Hanusch, F.; Bein, T.; Snaith, H. J.; Friend, R. H. *Nat. Nanotechnol.* **2014**, *9*, 687−692.
(16) Zhou, H.; Chen, Q.; Li, G.; Luo, S.; Song, T.; Duan, H.-S.; Hong, Z.; You, J.; Liu, Y.; Yang, Y. *Science* **2014**, *345*, 542−546.
(17) Correa Baena, J. P.; Steier, L.; Tress, W.; Saliba, M.; Neutzner, S.; Matsui, T.; Giordano, F.; Jacobsson, T. J.; Srimath Kandada, A. R.; Zakeeruddin, S. M.; Petrozza, A.; Abate, A.; Nazeeruddin, M. K.; Grätzel, M.; Hagfeldt, A. *Energy Environ. Sci.* **2015**, *8*, 2928−2934.
(18) Xiao, Z.; Kerner, R. A.; Zhao, L.; Tran, N. L.; Lee, K. M.; Koh, T.-W.; Scholes, G. D.; Rand, B. P. *Nat. Photonics* **2017**, *11*, 108−115.
(19) Kim, T. H.; Kim, S. G. *SH W* **2011**, *2*, 97−104.
(20) Tait, J.; Merckx, T.; Li, W.; Wong, C.; Gehlhaar, R.; Cheyns, D.; Turbiez, M.; Heremans, P. *Adv. Funct. Mater.* **2015**, *25*, 3393−3398.
(21) Gardner, L.; Tait, J.; Merckx, T.; Qiu, W.; Paetzold, U. W.; Kootstra, L.; Jaysankar, M.; Gehlhaar, R.; Cheyns, D.; Heremans, P.; Poortmans, J. *Adv. Energy Mater.* **2016**, *6*, 1600386.
(22) De Roo, J.; Ibáñez, M.; Geiregat, P.; Nedelcu, G.; Walravens, W.; Maes, J.; Martins, J. C.; Van Driessche, I.; Kovalenko, M. V.; Hens, Z. *ACS Nano* **2016**, *10*, 2071−2081.
(23) Palazon, F.; Almeida, G.; Akkerman, Q. A.; De Trizio, L.; Dang, Z.; Prato, M.; Manna, L. *Chem. Mater.* **2017**, *29*, 4167−4171.
(24) Liu, Z.; Bekenstein, Y.; Ye, X.; Nguyen, S. C.; Swabeck, J.; Zhang, D.; Lee, S. T.; Yang, P.; Ma, W.; Alivisatos, A. P. *J. Am. Chem. Soc.* **2017**, *139*, 5309−5312.
(25) Wu, L.; Zhong, Q.; Yang, D.; Chen, M.; Hu, H.; Pan, Q.; Liu, H.; Cao, M.; Xu, Y.; Sun, B.; Zhang, Q. *Langmuir* **2017**, *33*, 12689−12696.
(26) Tan, Y.; Zou, Y.; Wu, L.; Huang, Q.; Yang, D.; Chen, M.; Ban, M.; Wu, C.; Wu, T.; Bai, S.; Song, T.; Zhang, Q.; Sun, B. *ACS Appl. Mater. Interfaces* **2018**, *10*, 3784−3792.
(27) Wu, D. H.; Chen, A. D.; Johnson, C. S. *J. Magn. Reson., Ser. A* **1995**, *115*, 260−264.
(28) Wagner, R.; Berger, S. *J. Magn. Reson., Ser. A* **1996**, *123*, 119−121.
(29) ten Brinck, S.; Infante, I. *ACS Energy Lett.* **2016**, *1*, 1266−1272.
(30) Perdew, J. P.; Burke, K.; Ernzerhof, M. *Phys. Rev. Lett.* **1997**, *78*, 1396−1396.
(31) VandeVondele, J.; Hutter, J. *J. Chem. Phys.* **2007**, *127*, 114105.
(32) Hutter, J.; Iannuzzi, M.; Schiffmann, F.; Vandevondele, J. *Wiley Interdiscip. Rev. Comput. Mol. Sci.* **2014**, *4*, 15−25.
(33) Baranyi, A. D.; Onyszchuk, M.; Le Page, Y.; Donnay, G. *Can. J. Chem.* **1977**, *55*, 849−855.
(34) Zeldin, M.; Mehta, P.; Verngn, W. D. *Inorg. Chem.* **1979**, *18*, 463−466.
(35) Maciel, G. E.; James, R. V. *Inorg. Chem.* **1964**, *3*, 1650−1651.
(36) Jameson, C.; Mason, J. The Chemical Shift. In *Multinuclear NMR*; Mason, J., Ed.; Springer: 1987; pp 51−88.
(37) Hadzi, D.; Klofutar, C.; Oblak, S. *J. Chem. Soc. A* **1968**, *0*, 905−908.
(38) Murray, C. B.; Norris, D. J.; Bawendi, M. G. *J. Am. Chem. Soc.* **1993**, *115*, 8706−8715.
(39) Efros, A. L.; Rosen, M. *Annu. Rev. Mater. Sci.* **2000**, *30*, 475−521.
(40) Koole, R.; Groeneveld, E.; Vanmaekelbergh, D.; Meijerink, A.; De Mello Donega, C. Size Effects on Semiconductor Nanoparticles. In *Nanoparticles*; De Mello Donega, C., Ed.; Springer: 2014; pp 13−51.
(41) Green, M. L. H. *J. Organomet. Chem.* **1995**, *500*, 127−148.
(42) Shard, A. G. *Surf. Interface Anal.* **2014**, *46*, 175−185.
(43) Fritzinger, B.; Moreels, I.; Lommens, P.; Koole, R.; Hens, Z.; Martins, J. C. *J. Am. Chem. Soc.* **2009**, *131*, 3024−3032.

DOI: 10.1021/jacs.8b08978
J. Am. Chem. Soc. 2018, 140, 14878−14886